RESEARCH ARTICLE

In vivo supraspinatus muscle contractility and architecture in rabbit

Sydnee A. Hyman,[1,2] **Mackenzie B. Norman,**[2,3] **Shanelle N. Dorn,**[2] **Shannon N. Bremner,**[2]
Mary C. Esparza,[2] **Richard L. Lieber,**[4] **and Samuel R. Ward**[1,2,5]

[1]*Department of Bioengineering, University of California, San Diego, California;* [2]*Department of Orthopaedic Surgery, University of California, San Diego, California;* [3]*Dartmouth Geisel School of Medicine, Hanover, New Hampshire;* [4]*Shirley Ryan Ability Lab, Northwestern University, Chicago, Illinois;* and [5]*Department of Radiology, University of California, San Diego, California*

Hyman SA, Norman MB, Dorn SN, Bremner SN, Esparza MC, Lieber RL, Ward SR. In vivo supraspinatus muscle contractility and architecture in rabbit. *J Appl Physiol* 129: 1405–1412, 2020. First published October 8, 2020; doi:10.1152/japplphysiol.00609.2020.—The rotator cuff (RC) muscles are crucial in moving and stabilizing the glenohumeral joint, and tears can be functionally devastating. Chronic fatty and fibrotic muscle changes, which are nonresponsive to surgical tendon repair, are a focus of contemporary research. The rabbit model recapitulates key biological features of human RC tears, but function and physiology are poorly characterized; limited force and stress data are inconsistent with literature norms in other mammalian species. Here, we present an improved method to assess the physiology of the rabbit supraspinatus muscle (SSP), and we report values for healthy SSP architecture and physiology. Using female New Zealand White Rabbits ($n = 6$) under 2% isoflurane anesthesia, we surgically isolated the SSP and maximum isometric force measured at 4–6 muscle lengths. Architectural analysis was performed, and maximum isometric stress was computed. Whole muscle length-tension curves were generated using architectural measurements to compare experimental physiology to theoretical predictions. Maximum isometric force (80.87 ± 5.58 N) was dramatically greater than previous reports (11.06 and 16.1 N; $P < 0.05$). Architectural measurement of fiber length (34.25 ± 7.18 mm), muscle mass (9.9 ± 0.93 g), pennation angle ($23.67 \pm 8.32°$), and PCSA (2.57 ± 0.20 cm^2) were consistent with prior literature. Isometric stress (30.5 ± 3.07 N/cm^2) was greater than previous reports of rabbit SSP (3.10 and 4.51 N/cm^2), but similar to mammalian skeletal muscles (15.7–30.13 N/cm^2). Previous studies underestimated peak force by ~90%, which has profound implications for interpreting physiological changes as a function of disease state. The data that are presented here enable understanding the physiological implications of disease and repair in the RC of the rabbit.

NEW & NOTEWORTHY We introduce an improved method to assess rabbit supraspinatus muscle physiology. Maximum isometric force measured for the rabbit supraspinatus was dramatically greater than previous reports in the literature. Consequently, the isometric contractile stress reported is almost 10 times greater than previous reports of rabbit supraspinatus, but similar to available literature of other mammalian skeletal muscle. We show that previous reports of peak supraspinatus isometric force were subphysiological by ~90%

architecture; muscle force; muscle physiology; muscle stress; rotator cuff

INTRODUCTION

Chronic rotator cuff (RC) tendon tears are a common source of shoulder pathology, with a 30% prevalence above age 60 (2). RC tears can cause pain, tendon degeneration, tendon failure, and ultimately muscle retraction and atrophy, impairing function (13). The long-term sequela of muscle unloading and retraction appears to be muscle atrophy and fat accumulation (8, 16, 33), which is largely nonresponsive to rehabilitation (8, 39). While surgical tendon repair is common, decreased muscle quality (fibrosis, fatty infiltration, and atrophy) persists despite clinically successful repair and is correlated with poor functional outcomes (12).

Given the progressive pathophysiology of RC tears and the invasive methods needed to study them, it is difficult to study mechanisms of muscle atrophy and recovery in humans. While there has been a recent resurgence of small animal (mouse and rat) models of RC tears, the muscle phenotypes have limited severity, calling into question their utility as reasonable models of human muscle degeneration (6, 21, 25, 26). Some high-quality studies have been performed in sheep, which does recapitulate the persistent fatty atrophy seen in humans (8, 9). The rabbit model has emerged as an important animal model because, unlike rodent models, it recapitulates several important clinical characteristics of RC tear, such as muscle retraction, muscle atrophy, fatty infiltration, and inflammation with tenotomy alone (as opposed to tenotomy and denervation required in rodent models) (5, 7, 28, 35, 41). Animal models have been used to describe tear progression in many ways (fiber size, fatty infiltration, atrophy, and inflammation), and biological indicators of muscle function have been implicated in RC tears (membrane damage, fiber cytoskeletal disruption, extracellular matrix composition alteration, costamere structural disruption, and altered fiber morphology) (3, 14, 36, 37, 47).

However, surprisingly little attention has been paid to the physiological consequences of RC tears. Peak force and stress production are key variables, but muscle length-tension relationships are also important to muscle function because there is architectural evidence that retracted RC muscles experience serial sarcomere loss (11). This will have significant functional implications if the remaining sarcomeres are overstretched during surgical reattachment, and the reattached muscle is subsequently forced to operate on unusual portions of the length-tension curve (47). Despite this, few studies have measured contractile force and no studies have reported stress or the shape of the length-tension relationships for RC muscles. One study measured

Correspondence: S. R. Ward (s1ward@ucsd.edu).

supraspinatusp (SSP) contractile muscle force intraoperatively in human (10), one study reported infraspinatus contractile force in sheep (30), and two groups reported SSP contractile force in rabbit (4, 42). Importantly, contractile stress (calculated by dividing force by physiological cross-sectional area (PCSA) (27)) in these studies was low (3.10 and 4.51 N/cm^2) (4, 42) compared with available literature of other mammalian skeletal muscle (15.7 to 30.13 N/cm^2) (1, 34, 48). Given this large discrepancy, we believe the prior studies have underestimated the rabbit SSP maximum isometric force. On the basis of the reported value for SSP PCSA (2.8 cm^2) (27) and computing the average mammalian skeletal muscle specific tension from prior literature (22.8 ± 3.87 N/cm^2; $n = 80$) (1, 34), we expected SSP isometric contractile force to be ~64 N.

The primary purpose of this article is to describe the methods required to define maximum contractile force and stress values of rabbit SSP, and, secondarily, to quantify the length-tension relationship of the SSP in vivo. This should enable researchers assessing RC tear pathology to study functional outcomes and develop novel therapies.

MATERIALS AND METHODS

Surgical procedure. All experimental procedures were approved by the Institutional Animal Care and Use Committee (IACUC) of the University of California, San Diego. Six skeletally mature female New Zealand White rabbits (6 mo old, mean body wt: 4.3±0.3 kg) were used to determine the length-tension relationship for the SSP. Animal preparation for contractile testing was performed as described previously (48). Briefly, rabbits were anesthetized with a subcutaneous injection of a ketamine-xylazine cocktail (50 and 5 mg/kg body mass, respectively) and maintained on 2% isoflurane anesthesia. Heart rate and oxygen saturation were monitored (VetOx, Heska, Fort Collins, CO) throughout the test duration. An incision was made along the scapular spine to expose the superficial shoulder muscles. The SSP was exposed by dividing the middle trapezius and deltoid muscles to access the vertebral border of the scapula. The suprascapular nerve was isolated by blunt dissection around the anterior aspect of the SSP (29), and a cuff electrode (Pulsar 6Bp Stimulator; FHC, Bowdoinham, ME) was placed around the nerve for direct stimulation [see Fig. 1 of Winters et al. 2009 for image of electrode in use (48)]. Nerve isolation was confirmed by delivering twitch stimulations and visualizing supraspinatus contraction.

Suture markers were placed at the distal and proximal muscle-tendon junctions to define muscle length in the neutral position (shoulder joint at 90°). This was chosen to recapitulate the in vivo configuration of the rabbit in quiet standing. Additional suture markers were placed to identify lateral, middle, and medial fascicles of the posterior aspect of the SSP (Fig. 1A). Sutures were used as fiducial markers to determine muscle and fascicle shortening during contraction. Intact muscle length measurements were recorded using digital calipers (Mitutoyo, accuracy of 0.01 mm) at four joint angle positions (as determined by a goniometer): 60°, 90°, 120°, and 150°, representing the full range of glenohumeral flexion and extension. These measurements were used to
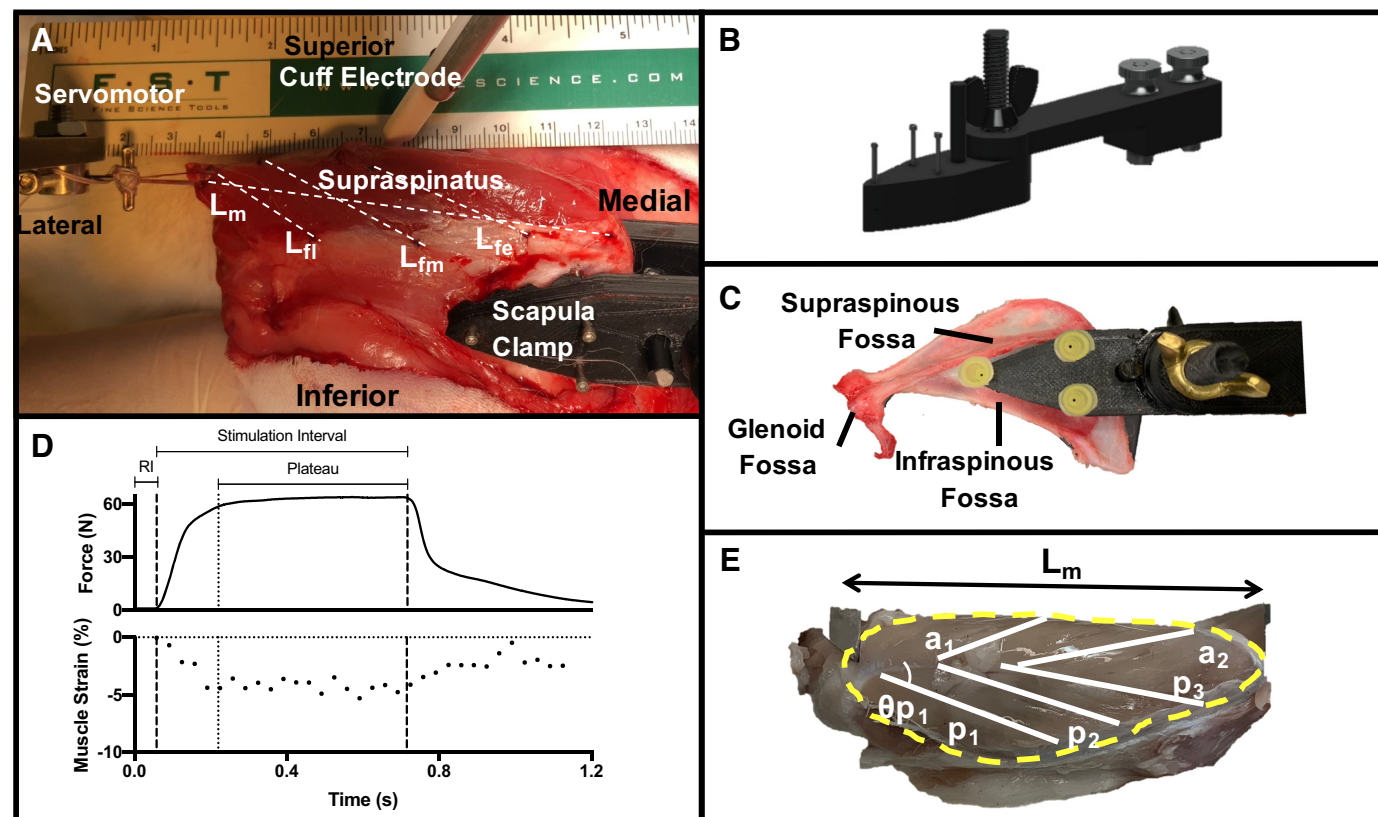

Fig. 1. Experimental setup (*A*) showing in vivo preparation of the scapula immobilized with the clamp attached, exposed supraspinatus muscle (SSP), and distal tendon attached with suture to the servomotor. Care was taken to ensure proper alignment of the tendon with axis of the motor. The cuff electrode is attached to the suprascapular nerve on the superior anterior aspect of the SSP. Dotted lines connect the suture markers indicating muscle length (L_m), lateral fascicle length (L_{fl}), mid-fascicle length (L_{fm}), and medial fascicle length (L_{fe}). CAD image of custom-made scapula clamp (*B*), illustrating the components required for assembly. Isolated scapula with clamp attached (*C*) to illustrate the position of scapula and clamp for experimentation. Representative traces (*D*) of force, and muscle strain during the nerve stimulation interval. The resting interval (RI) before contraction indicates when the resting muscle length is measured, and the plateau indicates where the peak isometric force and muscle strain are measured. Superior-inferior view of formalin-fixed SSP muscle, indicating the regions used for architectural analysis (*E*).
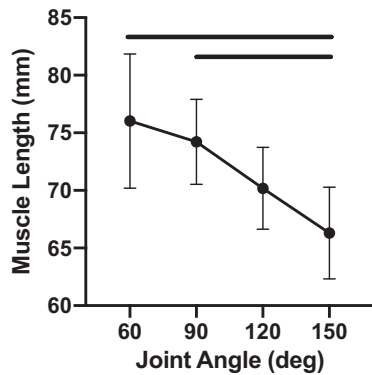
Fig. 2. Intact joint angle-muscle length measurements throughout full shoulder joint flexion/extension ($n = 6$ female rabbits). Muscle length was significantly shorter from 60° and 90° to 150° ($P < 0.05$ analyzed with ANOVA with post hoc Tukey test). Significance shown with horizontal lines. Points represent means ± SD.

correlate muscle length during contraction with the in vivo muscle operating range.

The distal SSP tendon was transected, released from the superior joint capsule, and sutured with two pieces of 2–0 Fiberwire (Arthrex, Naples, FL) using an infinity stitch and a modified Kessler stitch, both implemented to prevent suture slippage and tendon rupture. The suture was attached to a servomotor (Cambridge Model 310B; Aurora Scientific, Aurora, ON, Canada) and aligned with the force-generating axis of the motor. Muscle temperature was maintained at 37°C with radiant heat, heated saline, and a servo-temperature controller (Model 73A; Yellow Springs Instrument, Yellow Springs, OH). A custom-built clamp was used to immobilize the scapula, placed from the vertebral border along the scapular spine on top of the infraspinatus fossa (details below).

Scapula clamp manufacturing. The custom clamp used to stabilize the scapula was 3D printed (Creality Ender-3 Pro, Shenzhen Creality 3D Technology, Shenzhen, China) using ABS (32), with a layer height of 0.15 mm, a shell thickness of 1.2 mm, and 30% fill. They were reamed using a drill bits (3/8″ for large holes, 3/16″ for medium holes, and 1/16″ for small). Size 0 hex nuts were pressed into the hex indentations on the underside of the bottom piece of the clamp using a soldering iron, and then fixed into place using ABS cement (Oatey). A 0–80 screw was kept in the nut at all times to ensure that the holes didn't become obstructed. A two-inch piece of ABS rod stock (3/8″ diameter) was threaded with a 5/16–18 die, leaving about ¼″ unthreaded. The unthreaded end was cemented into the 3/8″ hole on the bottom piece of

the clamp with ABS cement and press down until flush with the underside. A one-inch piece of ABS rod stock (3/16″) was also cemented into the 3/16″ hole in the bottom piece of the clamp in a similar fashion, to stabilize the clamp while closed. The arm of the clamp was cemented to the top (flat) side of the top piece of the clamp, keeping the 3/8″ holes aligned. When the cement was fully cured, the clamp was assembled by putting the rods from the lower piece through their respective holes on the upper piece. The two pieces were secured with a 5/16-18 wing nut. The large holes on the mounting block were tapped with 10–32 threads, and the smaller holes were tapped with 4–40 threads (Fig. 1B). One-inch 10–32 screws were screwed through the holes on the mounting block, and the block was attached to a custom-machined adapter plate using 4–40 screws. The adapter plate was attached to an XZ axis rack and pinion stage (Edmund Optics, Barrington, NJ). The XZ stage was mounted onto an adjustable angle plate (ThorLabs, Newton, NJ) and set at a 30° angle to ensure the supraspinatus was contracting in a physiologically accurate direction. Three 1″ partially threaded 0–80 socket head screws were used to secure the nose of the clamp and ensure sufficient scapula stabilization. During the experiment, 20 gauge needles were used to create pilot holes through the infraspinous fossa of the scapula allowing screw placement through the bone. Figure 1C shows a rabbit scapula with soft tissue removed and needles inserted to illustrate the orientation.

Isometric length-tension protocol. The length-tension protocol consisted of a series of 100-Hz tetanic contractions (pulse width: 0.3 ms; amplitude: 10 V) over a 640-ms period. Two-minute rest intervals were imposed between contractions to minimize fatigue. The first contraction was performed with the muscle set to its neutral length (the muscle length measured at 90° joint angle). This was chosen as the starting length to ensure that the first contraction was performed at a relatively short muscle length, likely on the ascending limb of the length-tension curve (44). For each subsequent contraction, the servomotor position was advanced 5 mm to lengthen the muscle. Resting muscle length was measured between suture markers with calipers before each contraction during the resting interval (Fig. 1D), to ensure suture stretch was not included in the muscle length data for the length-tension curves. This process continued until muscle force dropped significantly, indicating that the muscle was operating on the descending limb of the length-tension curve, with a minimum of four contractions per animal. Force was acquired for each contraction using a data acquisition board (610E series; National Instruments, Austin, TX) and a custom-written LabView program (National Instruments) at 4 kHz per channel. Passive tension at each muscle length was obtained by measuring the baseline force. Net peak isometric force was defined as the difference between peak active tension during the plateau region (Fig. 1D) and passive tension. A typical experimental muscle force trace is shown in Fig. 1D. Note
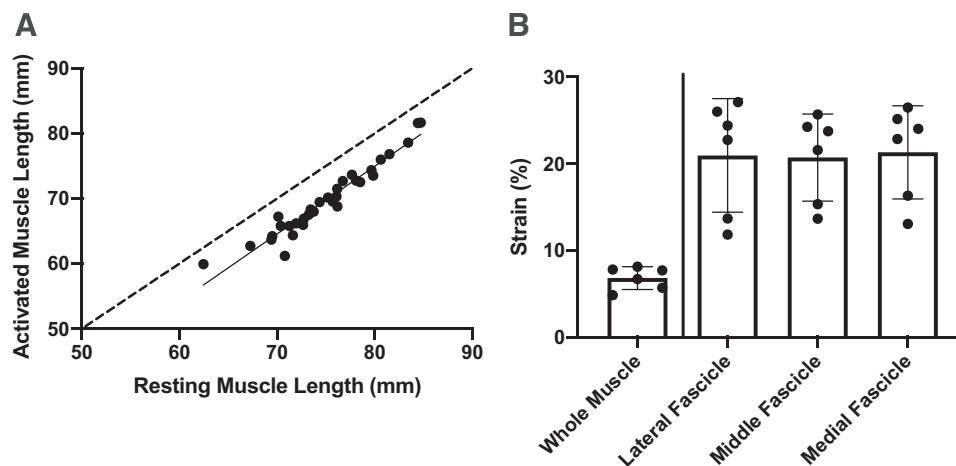

Fig. 3. Linear regression of activated versus resting muscle length (A) ($R^2 = 0.93$) with a line of identity (dashed), and each point representing one contraction ($n = 31$ contractions from six female rabbits). Average strains during contraction (B) for all contractions ($n = 31$ from six female rabbits) show that strains between fascicles are not significantly different, and fascicle strains are larger than whole muscle strain ($P < 0.05$; one-way ANOVA with post hoc Tukey test). Bars represent means ± SD.

the rapid tension rise and constant peak force clearly indicates that the muscle is contracting nearly isometrically.

Muscle and fascicle measurements. Videos of each contraction were taken at 1080-pixel resolution and 30 frames per second, and ImageJ software (38) was used to manually measure muscle and fascicle length in each frame. Activated muscle length was then computed from the measured muscle strain during the plateau region of each contraction (Fig. 1D). A representative plot of muscle length change during contraction is shown in Fig. 1D.

Muscle architecture measurements. After animals were euthanized, whole shoulders were fixed in 10% formalin in approximately the same orientation of 90° flexion to represent a neutral shoulder position. All architectural measurements were performed as previously described (11, 44). The supraspinatus was exposed by removing the superficial muscles (trapezius and deltoid), and several fascicles were marked: three regions posterior and two regions anterior (Fig. 1E). Muscle length and pennation angles of the marked fascicles were measured with digital calipers) before carefully removing the supraspinatus from the scapula. Muscle mass was recorded from fixed muscles, and fascicles were removed from distinct regions and measured for raw fiber length (27, 45). Subsequent sarcomere length measurements were performed using laser diffraction, as previously described (24). Individual muscle fibers were dissected from fascicles and mounted on glass slides. Sarcomere length was recorded for three individual fibers and averaged for each fascicle. Sarcomere number was calculated by dividing fiber length by sarcomere length. Physiological cross-sectional area (PCSA) was calculated using the formula:

$$PCSA = \frac{mass}{\rho * L_{fn}} \cos\theta$$

where density was assumed to be 1.056 g/cm^3 (45), L_{fn} is fiber length adjusted for sarcomere length, and θ is the average pennation angle for the muscle. One right side shoulder was damaged during sample preparation and discarded.

Theoretical length-tension curve. To reconcile experimental data with theoretical expectations for length-tension behavior, a length-tension curve was modeled using previously described methods (48). Briefly, a sarcomere level length-tension curve for rabbit skeletal muscle was generated: peak force was predicted at optimal sarcomere length (2.5 μm); the ascending limb started with minimum sarcomere length of 1.27 μm, and the zone of single overlap beginning at 1.70 μm (67.59% maximum force); the descending limb spanned from optimal length to maximum sarcomere length of 4.02 μm. The model was scaled from sarcomere to fiber level by multiplying sarcomere length values by serial sarcomere numbers. Then the model was scaled to the whole muscle level using architectural measurements from harvested supraspinatus muscles. This established the relationship between normalized fiber length (34.22 mm) and normalized muscle length (75.87 mm) from the average pennation angle (23.67°). The resting in vivo operating range for the SSP was determined using the intact muscle length-joint angle measurements, where the muscle length measured at maximum extension and maximum flexion set the lower and upper physiological limits for the muscle length range. The activated in vivo operating range was defined by scaling the resting muscle lengths by the average muscle strain during contraction.

Data analysis. Intact muscle length, strain, isometric tension, and isometric stress were analyzed using one-way ANOVA with post hoc Tukey test. Paired *t* tests were used to compare left versus right side architectural measurements. Two-way ANOVA with post hoc Tukey test was used to compare left versus right differences, and the Sidak test was used to compare regional differences for architecture. Linear regression was used to analyze the resting and activated muscle lengths. A one-sample *t*-test was used to compare peak force and stress values to individual literature values. Significance level was set at $P < 0.05$, and data are presented as means ± SD.

RESULTS

Intact joint angle-muscle length. The supraspinatus muscle length shortened (76.03 to 66.30 mm) as the glenohumeral joint
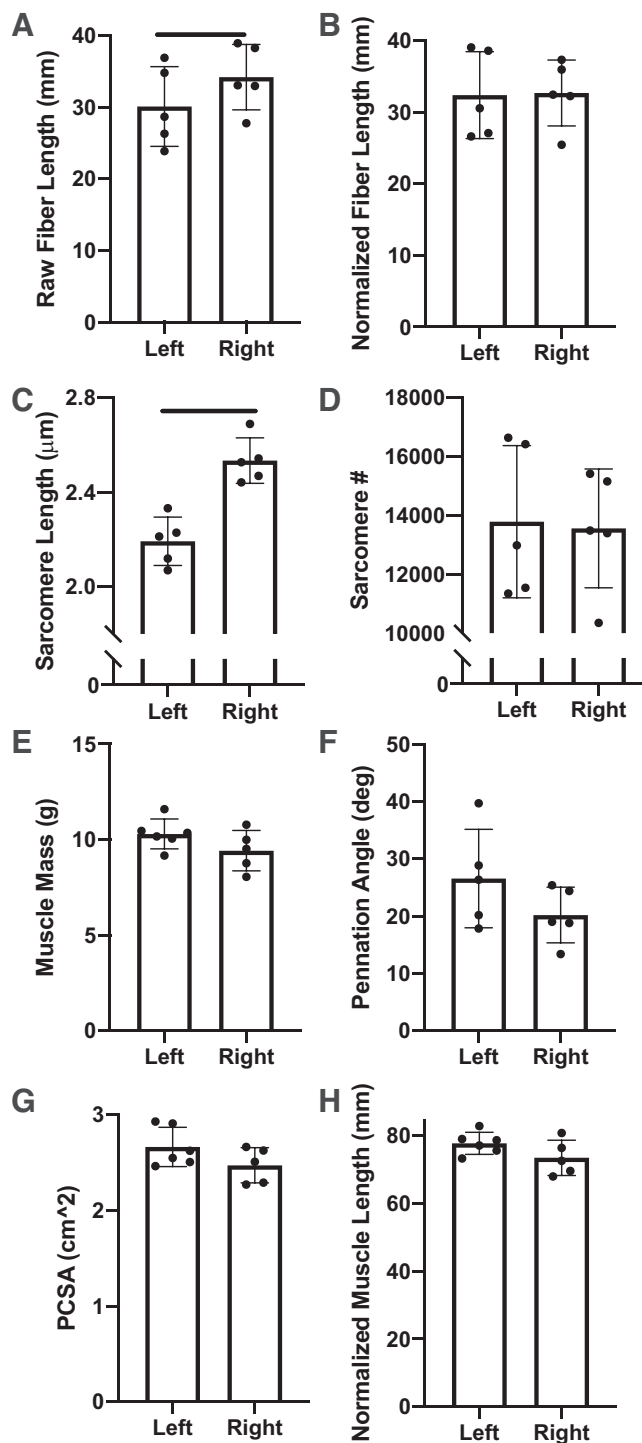

Fig. 4. Average architectural values for the left (n = 6 female rabbits) and right (n = 5 female rabbits) side supraspinatus muscles. Raw fiber length (A) and sarcomere length (C) were significantly shorter on the left side (P = 0.0453, P = 0.0005). Normalized fiber length (B), sarcomere number (D), muscle mass (E), pennation angle (F), physiological cross-sectional area (PCSA) (G), and normalized muscle length (H) were similar between left and right sides. Analyzed with paired *t* test. Bars represent means ± SD.

moved from 60° to 150° in flexion/extension (Fig. 2)—the dominant physiological plane and range limit in the rabbit. Muscle length at 60° and 90° was significantly longer ($P < 0.05$) than at 150° (full flexion). This length range represented the resting in vivo operating range for the muscle.

Muscle and fascicle strain. Strain for the whole muscle and three fascicles was measured during each contraction (from the resting length to the activated length during the plateau region of each contraction). A strong linear correlation ($r^2 = 0.93$) was observed between resting precontraction length and the activated length (Fig. 3A). Average muscle, lateral fascicle, mid-fascicle, and medial fascicle strains were measured over all contractions (6.8%, 20.95%, 20.7%, and 21.31%). Strains among fascicles were not significantly different (Fig. 3B) and were larger overall than whole muscle strain ($P < 0.05$). This is consistent with the behavior of a pennate muscle where small muscle strain corresponds to large fascicle strain.

Muscle architecture. Paired *t* tests were used to compare the left and right sides, with a total of five pairs of shoulders used, since one right side was lost during sample preparation. No significant differences were found between the left (experimental) and right (control) sides for normalized fiber length, sarcomere number, muscle mass, pennation angle, or PCSA (Fig. 4). Raw fiber length and sarcomere lengths between left and right were

significantly different ($P = 0.0453$, $P = 0.0005$, respectively), which was expected since the supraspinatus had been tenotomized immediately before physiology testing, causing mechanical unloading and subsequent muscle retraction.

Regionally, differences between left and right sides were the result of the transection of the tendon for performing the experiment (Fig. 5): the pennation angle was greater and raw fiber length nearest the myotendinous junction (P1) were shortened, and all sarcomere lengths except the A2 region were significantly shortened due to muscle recoil. Between regions, fiber lengths are significantly larger from lateral to medial (P1 vs. P3 and A1 vs. A2), while sarcomere lengths are not different. Pennation angles are smaller from lateral to medial, as the longer fibers align more closely with the force generating axis of the muscle. Statistical significance was determined from post hoc Tukey or Sidak tests with $P < 0.05$.

Theoretical length-tension curve. Experimental whole muscle length-tension curves are typically shaped as inverted parabolas (Fig. 6). Resting muscle length (Fig. 6A) is shifted right compared with activated muscle length (Fig. 6B) because the muscle shortens during contraction (22, 23, 40, 49). Activated muscle length is computed from the real-time muscle strain measurements during contraction. The in vivo operating range (shown as the solid line on both plots) encompasses the shallow
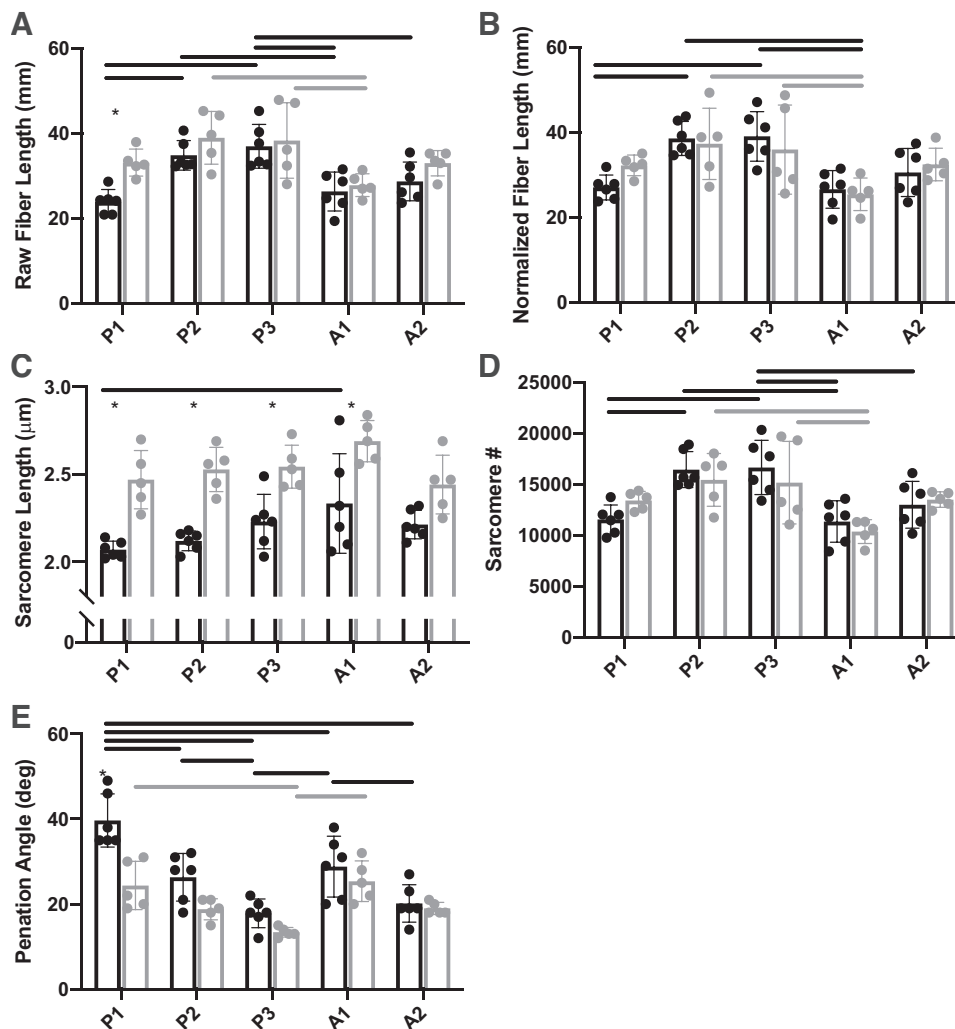

Fig. 5. Regional architectural measurements for rabbit supraspinatus muscle (SSP). Left (black circles; *n* = six female rabbits) and right (gray circles; *n* = 5 female rabbits) sides are shown for each muscle region (P1, P2, P3, A1, and A2). Two-way ANOVA with post hoc Tukey test and Sidak test was used to analyze left vs. right side and regional differences, respectively. Lines represent interregion differences (black lines for left side and gray lines for right side), and asterisks represent intraregion differences between left and right side. Raw fiber length (A), normalized fiber length (B), and sarcomere number (D), all show increases in the medial regions (P3 and A2) compared with the lateral regions (P1 and A1). The left side P1 region raw fiber length (A) was significantly shorter than right side, but after normalization (B) is not different. Sarcomere lengths were significantly different between sides in the P1, P2, P3, and A1 regions. Pennation angle (E) was significantly greater on left P1 region compared with right, and decreased moving from lateral to medial. These data are consistent with what is expected after the muscle is released at its tendinous insertion to the greater tubercle. Bars represent means ± SD; *$P < 0.05$.

Fig. 6. Predicted length-tension curves (dashed line) normalized to % of maximal isometric tension (P_0) for each rabbit. In vivo operating range shown as solid line. Resting muscle lengths were experimentally measured before each muscle contraction (*A*), while activated muscle lengths were computed using the measured muscle strain during the contraction plateau (*B*). The leftward shift of the activated muscle lengths highlights the importance of measuring the muscle length during contraction (activated), as opposed to before contraction (resting). Each point represents one contraction ($n = 31$), with different symbols used for each animal ($n = 6$ female rabbits).
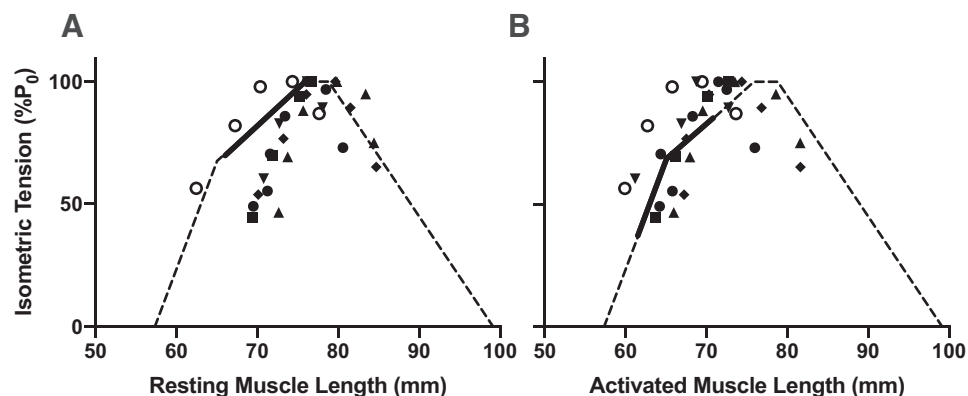
ascending limb for the resting length (Fig. 6*A*) but includes both ascending limbs for the activated length (Fig. 6*B*). This corresponds to a contractile force variation of ~30% at the resting muscle length and ~40% at the activated muscle length.

Maximum isometric force and stress. Experimentally measured maximum isometric force SSP production (80.87 ± 5.58 N) (Fig. 7*A*) was significantly greater compared with prior reports (11.06 ± 1.62 N and 16.1 ± 1.7 N; $P < 0.05$) (4, 43). Maximum stress (30.5 ± 3.07 N/cm^2) (Fig. 7*B*) was, therefore, significantly greater than SSP stress values that we calculated from the previously reported force measurements (3.01 and 4.51 N/cm^2; $P < 0.05$) (4, 43). However, measured stress was within the range of other mammalian skeletal muscles (range 15.7 to 30.13 N/cm^2) (1, 34).

DISCUSSION

The purpose of this study was to determine the maximum contractile force and stress and, secondarily, to understand the normal length-tension behavior for the rabbit SSP. We predicted the peak isometric tension using methods and architecture previously described (27, 48) to benchmark our experimental expectations. We measured maximum isometric force, which was significantly higher than previously described (4, 42). After performing a detailed architectural assessment of the SSP, we generated a theoretical length-tension curve to attempt to explain our experimental data based on classic muscle physiology (1). Using intact resting muscle length values and whole muscle contraction strain, we determined the in vivo operating range of the SSP. The activated muscle length-tension curve was computed by scaling resting muscle length by the strain decrease measured during contraction

and is shifted left compared with the resting muscle length-tension curve, as it incorporates muscle shortening with tendon elongation during contraction.

This is the first study to calculate the stress in rabbit SSP during maximal isometric contraction. Our predictions were based on the specific tension of mammalian skeletal muscle, 22.8 N/cm^2 (1, 34), since this was previously shown to correlate strongly with PCSA in rabbit hindlimb muscles (48). Although our stress value (30.5 ± 3.07 N/cm^2) was slightly higher than expected, it fell within the range reported in the literature (15.7 to 30.13 N/cm^2).

Architecturally, we report similar pennation angle and muscle lengths to prior studies, but longer fiber lengths and larger muscle mass (27). Consequently, PCSA values were lower in our study compared with prior literature. The increased muscle mass and animal size could explain the longer fiber lengths in our study, but these scaling relationships are not well understood. Architecturally, the gross anatomy and substructure is similar to the human SSP, as the regions of the muscle were subdivided according to prior work in human SSP architecture (44).

The predicted length-tension curve was fairly consistent with the resting muscle lengths, which are the typical muscle length measurements used (42, 48), but it was improved when using the activated muscle length, as the curve shifts to the left (Fig. 6). The rabbit SSP is highly pennate, contains a robust internal tendon, and has heterogeneous fiber lengths, all three factors of which complicate whole muscle modeling (15, 17, 20, 23, 31). However, the primary function of the model in this case was to determine the testing range for muscle lengths and provide a reasonable estimate of maximum contractile force, making it sufficient for the scope of this study.

The leftward shift for the activated muscle lengths is largely explained by the series compliance in the muscle-tendon unit
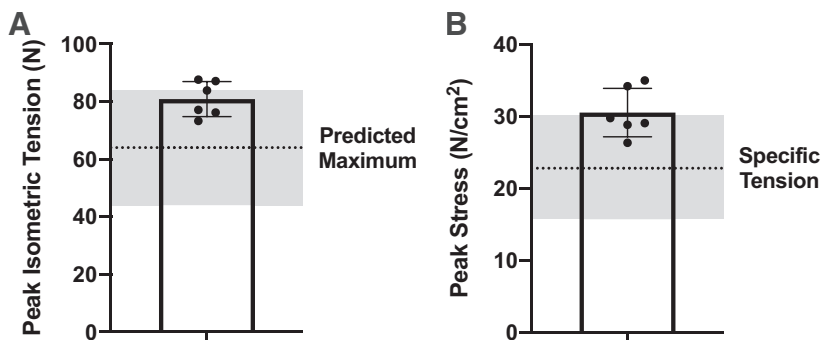

Fig. 7. Peak isometric tension (*A*) and stress (*B*) for our study ($n = 6$ female rabbits). Bars represent means $\pm$ SD. Gray bands represent the range of prior studies for muscle stress and corresponding predicted muscle force in mammalian skeletal muscle.

and muscle strain during contraction (22, 23, 40, 49). Whereas the muscle-tendon unit maintains a fixed length, the muscle shortens and tendon lengthens (22, 49). This is crucially important, as the resting muscle length cannot reliably be used to estimate contractile force generation in a muscle-tendon unit with a long and/or compliant tendon (46). If resting muscle length is used to predict optimal muscle length in this system, when the muscle strains early during contraction, the muscle will shorten against the lengthening tendon. As a result, the active tension measured with a resting muscle starting length would be a submaximal contraction (Fig. 1D). This is illustrated clearly over the ascending limbs of the length-tension curve: as the muscle shortens, force decreases. Given the average whole muscle strain of 6.8% during contraction, corresponding to a discrepancy in predicted force production of ~30–40%.

The force generation that we report is significantly higher than previously described (4, 42). There are several potential contributing factors to this discrepancy: Primarily, in previous studies, tetanic tension was recorded only at the muscle length that yielded the greatest twitch tension. However, because of the significant muscle strain during contraction, this would yield a submaximal tetanic tension because of the high series compliance in this system and the relatively brief "active state" of the twitch itself (18). Additionally, firmly fixing both ends of the system (the scapula and the released tendon) is challenging, and any movement in the system decreases the recorded force due to the drop in force that occurs as the muscle shortens (19). The relationship between resting length and optimal length varies on the basis of muscle and connective tissue anatomy in a muscle-specific and species-specific manner, suggesting that the resting muscle length is insufficient to measure maximal tension (1, 20, 22, 23, 40, 46). This is also the reason that we generated the entire length-tension curve so as not to assume the relationship between the two parameters for this muscle. Finally, isolating and reliably stimulating the suprascapular nerve can also prove challenging. The current study used female New Zealand White (NZW) rabbits with a mean body weight of 4.3 kg, whereas the previous studies used slightly smaller rabbits [Fabiś et al. (4) used 3–4 kg "mixed-race" males and Valencia et al. (42) used 2.3 kg NZW and did not indicate the sex of the animal]. Despite these differences, to our knowledge there are no differences in contractility based on sex for 6-mo-old rabbits, and there are no available published data regarding the growth curve for body weight versus SSP size. However, even if body weight and SSP size were to scale linearly, a 50% difference in body mass would correlate with a 50% difference in supraspinatus mass. With a 50% smaller muscle, we would expect roughly 50% lower force production, not the much greater 90% difference that we have observed.

This study has several limitations. First, interference from the infraspinatus (ISP), which is also innervated by the suprascapular nerve could theoretically increase our force recordings. We aimed to isolate the SSP by releasing the tendon lateral to medial (~1 cm) from the ISP tendon, but we did not surgically separate the muscle bellies of SSP and ISP. However, the scapular spine serves as a bony separation between SSP and ISP muscles, making direct force transmission from the ISP unlikely. Additionally, stress values are similar to the vast majority of other mammalian skeletal muscle reports (1, 34, 48). Taken together, we believe our values represent the SSP and not interference by the ISP. Because we believe we have completely separated the distal tendons, and lateral force transmission is negligible because

of the scapular spine, if release differences were contributing to measured force differences among the various studies, then other studies would have been reporting higher, not lower, forces. However, when we test the muscles at a short resting length, we get similar results to the other studies. This is why testing at multiple muscle lengths (especially longer lengths) is important to ensure the maximum isometric forces are captured. This is uniquely important in the rabbit SSP system because significant shortening strains are observed in the muscle-tendon unit, even when the bones are adequately secured. Second, we assume that our maximum recorded force is on the plateau of the length-tension curve for each rabbit, which could produce a shift in the curve. Third, we did not measure real-time changes in sarcomere length during contractions, and thus, we can only make indirect correlations to the physiological operating range of the SSP through intact muscle length-joint angle relationships and measured muscle strain during contraction. Lastly, the modeling strategy that we employed was developed for hindlimb muscles, not highly pennate muscles with high series elasticity, potentially influencing the accuracy of the model.

In summary, this study describes the methods to isolate the rabbit supraspinatus, immobilize the scapula, and perform physiological testing to assess its length-tension relationship. We report the maximum contractile force generation for the muscle and a detailed architectural analysis, allowing for computation of muscle stress. These methods will be useful for future investigations into the physiological effects of rotator cuff tear and subsequent repair in animal systems, which is clinically valuable (9, 10, 16, 43).

DISCLOSURES

No conflicts of interest, financial or otherwise, are declared by the authors.

AUTHOR CONTRIBUTIONS

S.A.H. and S.R.W. conceived and designed research; S.A.H., M.B.N., S.N.D., S.N.B., M.C.E., and S.R.W. performed experiments; S.A.H., M.B.N., S.N.D., and S.N.B. analyzed data; S.A.H. and S.R.W. interpreted results of experiments; S.A.H. prepared figures; S.A.H. and S.N.B. drafted manuscript; S.A.H., R.L.L., and S.R.W. edited and revised manuscript; S.A.H., M.B.N., S.N.D., S.N.B., M.C.E., R.L.L., and S.R.W. approved final version of manuscript.

REFERENCES

1. **Close RI.** Dynamic properties of mammalian skeletal muscles. *Physiol Rev* 52: 129–197, 1972. doi:10.1152/physrev.1972.52.1.129.

2. **Collin P, Thomazeau H, Walch G, Gerber C, Mansat P, Favard L, Colmar M, Kempf JF, Hervé A, Betz M.** Clinical and structural outcome twenty years after repair of isolated supraspinatus tendon tears. *J Shoulder Elbow Surg* 28: 196–202, 2019. doi:10.1016/j.jse.2018.07.023.

3. **Davis ME, Stafford PL, Jergenson MJ, Bedi A, Mendias CL.** Muscle fibers are injured at the time of acute and chronic rotator cuff repair. *Clin Orthop Relat Res* 473: 226–232, 2015. doi:10.1007/s11999-014-3860-y.

4. **Fabiś J, Kordek P, Bogucki A, Mazanowska-Gajdowicz J.** Function of the rabbit supraspinatus muscle after large detachment of its tendon: 6-week, 3-month, and 6-month observation. *J Shoulder Elbow Surg* 9: 211–216, 2000. doi:10.1067/mse.2000.105134.

5. **Farshad M, Meyer DC, Nuss KMR, Gerber C.** A modified rabbit model for rotator cuff tendon tears: functional, histological and radiological characteristics of the supraspinatus muscle. *Shoulder Elbow* 4: 90–94, 2012. doi:10.1111/j.1758-5740.2011.00170.x.

6. **Farshad M, Würgler-Hauri CC, Kohler T, Gerber C, Rothenfluh DA.** Effect of age on fatty infiltration of supraspinatus muscle after experimental tendon release in rats. *BMC Res Notes* 4: 530, 2011. doi:10.1186/1756-0500-4-530.

7. **Gerber C, Meyer DC, Nuss KM, Farshad M.** Anabolic steroids reduce muscle damage caused by rotator cuff tendon release in an experimental study in rabbits. *J Bone Joint Surg Am* 93: 2189–2195, 2011. doi:10.2106/JBJS.J.01589.

8. **Gerber C**, **Meyer DC**, **Schneeberger AG**, **Hoppeler H**, **von Rechenberg B.** Effect of tendon release and delayed repair on the structure of the muscles of the rotator cuff: an experimental study in sheep. *J Bone Joint Surg Am* 86: 1973–1982, 2004. doi:10.2106/00004623-200409000-00016.

9. **Gerber C**, **Schneeberger AG**, **Beck M**, **Schlegel U.** Mechanical strength of repairs of the rotator cuff. *J Bone Joint Surg Br* 76: 371–380, 1994. doi:10.1302/0301-620X.76B3.8175836.

10. **Gerber C**, **Schneeberger AG**, **Hoppeler H**, **Meyer DC.** Correlation of atrophy and fatty infiltration on strength and integrity of rotator cuff repairs: a study in thirteen patients. *J Shoulder Elbow Surg* 16: 691–696, 2007. doi:10.1016/j.jse.2007.02.122.

11. **Gibbons MC**, **Sato EJ**, **Bachasson D**, **Cheng T**, **Azimi H**, **Schenk S**, **Engler AJ**, **Singh A**, **Ward SR.** Muscle architectural changes after massive human rotator cuff tear. *J Orthop Res* 34: 2089–2095, 2016. doi:10.1002/jor.23256.

12. **Gladstone JN**, **Bishop JY**, **Lo IKY**, **Flatow EL.** Fatty infiltration and atrophy of the rotator cuff do not improve after rotator cuff repair and correlate with poor functional outcome. *Am J Sports Med* 35: 719–728, 2007. doi:10.1177/0363546506297539.

13. **Goutallier D**, **Postel J-M**, **Gleyze P**, **Leguilloux P**, **Van Driessche S.** Influence of cuff muscle fatty degeneration on anatomic and functional outcomes after simple suture of full-thickness tears. *J Shoulder Elbow Surg* 12: 550–554, 2003. doi:10.1016/S1058-2746(03)00211-8.

14. **Gumucio JP**, **Davis ME**, **Bradley JR**, **Stafford PL**, **Schiffman CJ**, **Lynch EB**, **Claflin DR**, **Bedi A**, **Mendias CL.** Rotator cuff tear reduces muscle fiber specific force production and induces macrophage accumulation and autophagy. *J Orthop Res* 30: 1963–1970, 2012. doi:10.1002/jor.22168.

15. **Herring SW**, **Grimm AF**, **Grimm BR.** Functional heterogeneity in a multipinnate muscle. *Am J Anat* 154: 563–575, 1979. doi:10.1002/aja.1001540410.

16. **Hersche O**, **Gerber C.** Passive tension in the supraspinatus musculotendinous unit after long-standing rupture of its tendon: a preliminary report. *J Shoulder Elbow Surg* 7: 393–396, 1998. doi:10.1016/S1058-2746(98)90030-1.

17. **Herzog W**, **ter Keurs HEDJ.** Force-length relation of in-vivo human rectus femoris muscles. *Pflugers Arch* 411: 642–647, 1988. doi:10.1007/BF00580860.

18. **Hill AV.** The mechanics of active muscle. *Proc R Soc Lond Ser B* 141: 104–117, 1953. doi:10.1098/rspb.1953.0027.

19. **Hill AV.** The effect of load on the heat of shortening of muscle. *Proc R Soc Lond B Biol Sci* 159: 297–318, 1964. doi:10.1098/rspb.1964.0004.

20. **Kawakami Y**, **Lieber RL.** Interaction between series compliance and sarcomere kinetics determines internal sarcomere shortening during fixed-end contraction. *J Biomech* 33: 1249–1255, 2000. doi:10.1016/S0021-9290(00)00095-6.

21. **Kim HM**, **Galatz LM**, **Lim C**, **Havlioglu N**, **Thomopoulos S.** The effect of tear size and nerve injury on rotator cuff muscle fatty degeneration in a rodent animal model. *J Shoulder Elbow Surg* 21: 847–858, 2012. doi:10.1016/j.jse.2011.05.004.

22. **Lieber RL**, **Brown CG**, **Trestik CL.** Model of muscle-tendon interaction during frog semitendinosis fixed-end contractions. *J Biomech* 25: 421–428, 1992. doi:10.1016/0021-9290(92)90261-X.

23. **Lieber RL**, **Leonard ME**, **Brown CG**, **Trestik CL.** Frog semitendinosis tendon load-strain and stress-strain properties during passive loading. *Am J Physiol Cell Physiol* 261: C86–C92, 1991. doi:10.1152/ajpcell.1991.261.1.C86.

24. **Lieber RL**, **Yeh Y**, **Baskin RJ.** Sarcomere length determination using laser diffraction. Effect of beam and fiber diameter. *Biophys J* 45: 1007–1016, 1984. doi:10.1016/S0006-3495(84)84246-0.

25. **Liu X**, **Laron D**, **Natsuhara K**, **Manzano G**, **Kim HT**, **Feeley BT.** A mouse model of massive rotator cuff tears. *J Bone Joint Surg Am* 94: e41, 2012. doi:10.2106/JBJS.K.00620.

26. **Liu X**, **Manzano G**, **Kim HT**, **Feeley BT.** A rat model of massive rotator cuff tears. *J Orthop Res* 29: 588–595, 2011. doi:10.1002/jor.21266.

27. **Mathewson MA**, **Kwan A**, **Eng CM**, **Lieber RL**, **Ward SR.** Comparison of rotator cuff muscle architecture between humans and other selected vertebrate species. *J Exp Biol* 217: 261–273, 2014. doi:10.1242/jeb.083923.

28. **Matsumoto F**, **Uhthoff HK**, **Trudel G**, **Loehr JF.** Delayed tendon reattachment does not reverse atrophy and fat accumulation of the supraspinatus—an experimental study in rabbits. *J Orthop Res* 20: 357–363, 2002. doi:10.1016/S0736-0266(01)00093-6.

29. **McCracken TO**, **Kainer RA**, **Carlson D.** Color Atlas of Small Animal Anatomy: The Essentials, *Revised Edition* [Online]. https://www.wiley.com/en-us/Color+Atlas+of+Small+Animal+Anatomy%3A+The+Essentials%2C+Revised+Edition-p-9780813816081 [24 Aug 2020].

30. **Meyer DC**, **Gerber C**, **Von Rechenberg B**, **Wirth SH**, **Farshad M.** Amplitude and strength of muscle contraction are reduced in experimental tears of the rotator cuff. *Am J Sports Med* 39: 1456–1461, 2011. doi:10.1177/0363546510396305.

31. **Morgan DL.** From sarcomeres to whole muscles. *J Exp Biol* 115: 69–78, 1985.

32. **Muscle Physiology Lab.** Rabbit Scapula Clamp [Online]. UC San Diego. http://muscle.ucsd.edu/projects/downloads.shtml.

33. **Petersen SA**, **Murphy TP.** The timing of rotator cuff repair for the restoration of function. *J Shoulder Elbow Surg* 20: 62–68, 2011. doi:10.1016/j.jse.2010.04.045.

34. **Powell PL**, **Roy RR**, **Kanim P**, **Bello MA**, **Edgerton VR.** Predictability of skeletal muscle tension from architectural determinations in guinea pig hindlimbs. *J Appl Physiol* 57: 1715–1721, 1984. doi:10.1152/jappl.1984.57.6.1715.

35. **Rubino LJ**, **Stills HF Jr**, **Sprott DC**, **Crosby LA.** Fatty infiltration of the torn rotator cuff worsens over time in a rabbit model. *Arthroscopy* 23: 717–722, 2007. doi:10.1016/j.arthro.2007.01.023.

36. **Ruoss S**, **Möhl CB**, **Benn MC**, **von Rechenberg B**, **Wieser K**, **Meyer DC**, **Gerber C**, **Flück M.** Costamere protein expression and tissue composition of rotator cuff muscle after tendon release in sheep. *J Orthop Res* 36: 272–281, 2018. doi:10.1002/jor.23624.

37. **Sato EJ**, **Killian ML**, **Choi AJ**, **Lin E**, **Esparza MC**, **Galatz LM**, **Thomopoulos S**, **Ward SR.** Skeletal muscle fibrosis and stiffness increase after rotator cuff tendon injury and neuromuscular compromise in a rat model. *J Orthop Res* 32: 1111–1116, 2014. doi:10.1002/jor.22646.

38. **Schindelin J**, **Arganda-Carreras I**, **Frise E**, **Kaynig V**, **Longair M**, **Pietzsch T**, **Preibisch S**, **Rueden C**, **Saalfeld S**, **Schmid B**, **Tinevez J-Y**, **White DJ**, **Hartenstein V**, **Eliceiri K**, **Tomancak P**, **Cardona A.** Fiji: an open-source platform for biological-image analysis. *Nat Methods* 9: 676–682, 2012. doi:10.1038/nmeth.2019.

39. **Shen P-H**, **Lien S-B**, **Shen H-C**, **Lee C-H**, **Wu S-S**, **Lin L-C.** Long-term functional outcomes after repair of rotator cuff tears correlated with atrophy of the supraspinatus muscles on magnetic resonance images. *J Shoulder Elbow Surg* 17, Suppl: 1S–7S, 2008. doi:10.1016/j.jse.2007.04.014.

40. **Trestik CL**, **Lieber RL.** Relationship between Achilles tendon mechanical properties and gastrocnemius muscle function. *J Biomech Eng* 115: 225–230, 1993. doi:10.1115/1.2895479.

41. **Uhthoff HK**, **Matsumoto F**, **Trudel G**, **Himori K.** Early reattachment does not reverse atrophy and fat accumulation of the supraspinatus—an experimental study in rabbits. *J Orthop Res* 21: 386–392, 2003. doi:10.1016/S0736-0266(02)00208-5.

42. **Valencia AP**, **Iyer SR**, **Pratt SJP**, **Gilotra MN**, **Lovering RM.** A method to test contractility of the supraspinatus muscle in mouse, rat, and rabbit. *J Appl Physiol (1985)* 120: 310–317, 2016. doi:10.1152/japplphysiol.00788.2015.

43. **Valencia AP**, **Lai JK**, **Iyer SR**, **Mistretta KL**, **Spangenburg EE**, **Davis DL**, **Lovering RM**, **Gilotra MN.** Fatty infiltration is a prognostic marker of muscle function after rotator cuff tear. *Am J Sports Med* 46: 2161–2169, 2018. doi:10.1177/0363546518769267.

44. **Ward SR**, **Hentzen ER**, **Smallwood LH**, **Eastlack RK**, **Burns KA**, **Fithian DC**, **Friden J**, **Lieber RL.** Rotator cuff muscle architecture: implications for glenohumeral stability. *Clin Orthop Relat Res* 448: 157–163, 2006. doi:10.1097/01.blo.0000194680.94882.d3.

45. **Ward SR**, **Lieber RL.** Density and hydration of fresh and fixed human skeletal muscle. *J Biomech* 38: 2317–2320, 2005. doi:10.1016/j.jbiomech.2004.10.001.

46. **Ward SR**, **Loren GJ**, **Lundberg S**, **Lieber RL.** High stiffness of human digital flexor tendons is suited for precise finger positional control. *J Neurophysiol* 96: 2815–2818, 2006. doi:10.1152/jn.00284.2006.

47. **Ward SR**, **Sarver JJ**, **Eng CM**, **Kwan A**, **Würgler-Hauri CC**, **Perry SM**, **Williams GR**, **Soslowsky LJ**, **Lieber RL.** Plasticity of muscle architecture after supraspinatus tears. *J Orthop Sports Phys Ther* 40: 729–735, 2010. doi:10.2519/jospt.2010.3279.

48. **Winters TM**, **Takahashi M**, **Lieber RL**, **Ward SR.** Whole muscle length-tension relationships are accurately modeled as scaled sarcomeres in rabbit hindlimb muscles. *J Biomech* 44: 109–115, 2011. doi:10.1016/j.jbiomech.2010.08.033.

49. **Zajac FE.** Muscle and tendon: properties, models, scaling, and application to biomechanics and motor control. *Crit Rev Biomed Eng* 17: 359–411, 1989.